KREOSUS: Technical Design Report

Şahinbey Zağanos UAV Team
Türkiye | Technical Design Report | 29 July 2026

***Abstract*—Storm Response requires one aircraft to deploy rapidly, map damage, locate targets, deliver aid, and recover within one mission clock. Kreosus links each scored phase and critical interface to measured, modeled, software, or analytical evidence. The 4.922 kg quadrotor fits an $18 \times 14 \times 8$ in Personal Item and was assembled without tools in a 147.5 s mean over ten trials. A disclosed 100,000-trial gated mission model completed within 45 min in all trials. The lap-nine gate authorized lap ten in 99.37% of trials; P95 mission time and energy were 40.37 min and 535.5 Wh, leaving 63.9 Wh, or 10.7%. At hover, the MAD 7005 with a 24×7.2 in propeller produced 1,230 gf at 85.0 W, or 14.47 gf/W. A 150 ft AGL mapping sortie produced an 84-image stitched risk map and detected all three planted targets. On 87 labeled instances collected during actual 150 ft AGL flight testing, RF-DETR Nano achieved 96.4% precision and 92.0% recall at 118 ms. Under full mission network load, LTE transferred all 84 images without loss and reached 1.18 s P95 exposure-to-release-intent latency. DROP-001 comprised 60 autonomous releases from RTK hover above 150 ft AGL in 2 m/s to 8 m/s winds; all 60 landed within 50 ft, with a 4.2 m mean radial error, 8.4 m maximum error, 100% object survival, and 100% channel match. Orthotropic bonded FEA returned a minimum directional factor of safety of approximately 2.0.**

***Index Terms*—storm response, mission optimization, image stitching, RF-DETR, RTK, rapid deployment, controlled delivery**

Acknowledgments—We thank our advisor and mentor Ertuğ Gözaydın for sustaining Team Zağanos for six years, and our advisor team for introducing us to SUAS. We thank Onshape for educational licenses and SimScale for simulation support. Şahinbey Municipality, Mayor Mehmet Tahmazoğlu, and Director Mustafa Said Çakallı provided primary material support. Salihli District Governor Ali Güldoğan, Buket Elmacı, Yasin Sarı, and Salihli Youth Center expanded local opportunities and provided workshop space. TÜBİTAK and the Ministry of Youth and Sports supported transportation. Erdal Rulman and Sefa Civata supplied essential hardware on short notice.

I. Competition Strategy

A. Storm-Response Score Architecture

The 2026 scenario follows the sequence required after a severe storm: rapid deployment, damage mapping, target detection, controlled aid delivery, and safe recovery [1]. Kreosus therefore uses one nominal mission plan: tool-free setup; autonomous takeoff; a gated endurance phase; one combined mapping and search pass; automatic target tracking and delivery-order evaluation; controlled delivery of water to the mannequin and a beacon to the tent; and autonomous landing. The nominal plan targets ten laps. A nine-lap fallback protects mapping and delivery when the lap-nine gate is not satisfied.

Exactly two people communicate during flight. The Safety Pilot maintains visual line of sight, takeover authority, and abort responsibility. The GCS Operator monitors QGroundControl, RTK state, battery, geofence, RC/SiK/LTE health, and payload status. An RTX 3050 ground workstation detects and tracks targets, evaluates delivery order, and generates release intents. Manual target selection is disabled while the aircraft is armed. This preserves the role boundary required for the 200-point operator category [1].

TABLE I
Nominal Score Target

Category	Basis	Target
Flight Endurance	10 laps plus autonomous takeoff/landing	250
Efficient Operators	Safety Pilot plus GCS Operator	200
Rapid Response	weight, Personal Item, tool-free, 6×99.9 Wh	200
Risk Mapping	150 ft AGL, 84-image stitched risk map	150
Search, Detect, Deliver	water to mannequin; beacon to tent	200
Mission target	all selected categories	**1000**

B. Gated Endurance Plan

MC-001 uses 100,000 trials and seed 260729. Effective lap speed follows a clipped normal distribution with a 18.0 m/s mean, 0.5 m/s standard deviation, and 16.5 m/s to 19.0 m/s bounds. All phase durations, phase powers, and the environmental multiplier are sampled together; late and high-consumption trials remain in the distribution. The gated mission completed within 45 min in 100,000 of 100,000 trials. The lap-nine gate authorized lap ten in 99.37% of trials; the remaining 0.63% transitioned directly from lap nine to mapping. P50/P95/P99 mission times are 38.82/40.37/41.02 min. Corresponding energy values are 487.3/535.5/554.5 Wh.

The team-set gate starts lap ten only when elapsed time is no more than 29:30, measured remaining energy is at least 150 Wh, and the current state predicts touchdown by 42:00. A failed predicate sends Kreosus directly to mapping after lap nine. These thresholds preserve time for both deliveries; they are not presented as a mathematically unique optimum.

C. Requirements and Trade Studies

The baseline records rejected alternatives as explicitly as selected hardware. Each decision is tied to score effect, failure surfaces, and verification burden rather than presented as a component catalog [2].

TABLE II
COMPETITION REQUIREMENTS AND TEAM VERIFICATION THRESHOLDS

ID	Competition requirement	Team-derived verification threshold	Evidence
OPS	Two flight operators; no secondary task during flight	Safety Pilot and GCS Operator only; manual target selection disabled while armed	documented role boundary and input policy
RAP	Personal Item, tool-free setup, full weight score threshold; each pack < 100 Wh	ready ≤ 180 s; 4.922 kg; 6×99.9 Wh	DEP-001: 10/10
END	Takeoff, gated endurance plan, mapping, delivery, and landing within Mission Time	nominal 10 laps; gated 9-lap fallback; 19.0 m/s ceiling; touchdown ≤ 42 min prediction; P95 reserve $\geq 10\%$	MC-001: 100% within 45 min; lap ten 99.37%; P95 40.37 min and 535.5 Wh
MAP	Produce a stitched Risk Map	84-image mapping sequence at 150 ft AGL; modeled coverage $\geq 98\%$; stitched orthomosaic produced	MAP-001 in Fig. 3; COM-001 transferred 84/84 images
DET	Detect mannequin and tent	precision $\geq 95\%$; recall $\geq 90\%$; actual 150 ft AGL flight-test data	DET-001: 96.4%; 92.0%; 118 ms
COM	Transport mission imagery and release intents	zero image loss in tested sequence; exposure-to-intent P95 ≤ 1.2 s	COM-001: 84/84; queue 3; P95 1.18 s
DEL	Deliver the correct aid object to the corresponding target	no uncontrolled release; 50 ft radius; correct channel; payload survives	DROP-001: 60/60 within 50 ft; 100% channel match and survival
STR	Safe airframe	orthotropic directional factor of safety ≥ 2.0	FEA-01/02

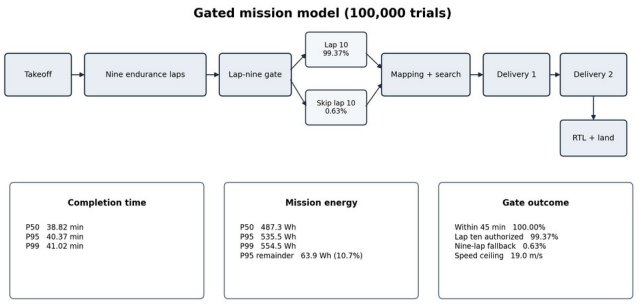

Fig. 1. All 100,000 gated mission trials completed within 45 min. Lap ten was authorized in 99.37% of trials, while 0.63% used the nine-lap fallback. P95 completion was 40.37 min, and 63.9 Wh, or 10.7%, remained at P95 consumption.

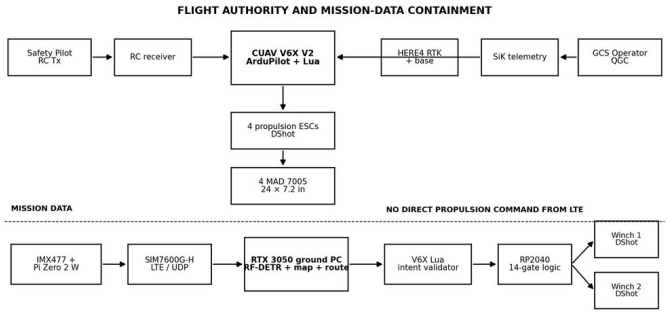

Fig. 2. The RC receiver and HERE4 feed the V6X independently. The V6X alone commands the four propulsion ESCs by DShot. LTE carries imagery and signed mission intents, which remain subject to V6X and RP2040 local gates.

TABLE III
HIGH-VALUE TRADE DECISIONS

Decision	Rejected alternative	Reason retained
Gated 10-lap plan; 9-lap fallback	fixed 7–8 laps	targets full endurance score while protecting mapping and delivery
One RTX 3050 workstation	onboard Jetson or third operator	removes airborne GPU mass and preserves two-operator score
RF-DETR Nano	YOLO11n / GroundingDINO	+12.9 pp precision and +10.4 pp recall for +5 ms versus YOLO total
Two independent winches	one shared mechanism	one jam cannot remove both delivery opportunities
Keyed removable arms plus QAD	folding hinges	same packing benefit without permanent hinge play
LTE plus local RC/SiK	LTE-only command	bandwidth without public-network flight dependence

II. DESIGN STRATEGY

A. Flight Architecture and Failure Containment

The CUAV V6X V2 was selected over lighter single-IMU controllers because its redundant inertial and barometric sensing, together with separated I/O, reduces common-cause loss of flight control [4]. HERE4 RTK provides the navigation and hover state used by the flight controller and local release gates [5]. A V6X Lua validator checks source, mission, monotonic sequence, CRC, time-to-live, geofence, EKF/RTK state, position, velocity, and altitude before it permits the RP2040 payload controller to proceed. If LTE is delayed or unavailable, no delivery intent is independently authorized; if the RTK, position, speed, altitude, or geofence predicates fail, the release gate remains closed and the aircraft can be recovered or aborted under Safety Pilot authority. The Pi Zero 2 W captures images, timestamps them, buffers data, and transports it over LTE; it does not command propulsion [6], [7], [8]. All six AM32 ESCs use bidirectional DShot, while PWM is limited to the two mechanical spool stops [3], [19].

B. Rapid-Response Airframe, Mass, and CG

The center chassis is a single PETG-CF print. It combines the battery bay, avionics shelf, arm sockets, landing interfaces, and payload guides, which removes plate-to-plate fasteners and shortens setup. PETG-CF was retained for impact tolerance and interlayer toughness supported by short-fiber PETG characterization [18]. Motor mounts and both spools use ASA-CF08 because they see the measured 65 °C motor environment, bearing and gear loads, weather exposure, and tighter creep requirements [9], [10]. Removable arms seat against shoulders and are retained by grooved cross-pins and clips. Q2434 quick-attach adapters remove all four propellers without tools [20].

The payload channels straddle the centerline and remain close to the vehicle CG. CAD mass properties across both-loaded, water-only, beacon-only, and empty states place the

TABLE IV
MEASURED MASS AND PAYLOAD-CG CLOSURE

Measured configuration	Mass / result	Closure
Dry aircraft: propulsion, arms, printed body, avionics, camera/LTE, winches, wiring	2,612 g	scale-closed without batteries or aid objects
Six separately packaged 99.9 Wh modules	1,900 g	599.4 Wh total; 6S in flight
Water payload	255 g	mannequin channel
Beacon payload	155 g	tent channel
Competition takeoff mass	4,922 g	10.85 lb; full weight score threshold
CAD payload-state CG envelope	$\leq$ 6.2 mm lateral	no observed hover-trim change in DROP-001
Personal Item to ready, $n = 10$	147.5 s mean; 157.8 s P95; 160 s worst	10/10 under 180 s; no tools

TABLE V
PROPULSION TRADE AND OPERATING POINTS

Candidate	Hover/packing assessment	Decision
MAD 5008 EEE	lower installed mass; less high-speed and wind margin	rejected
MAD M6C06 EEE V3	adequate curve and margin; weaker packing/test evidence	rejected
MAD 7005 EEE 230KV	14.47 gf/W hover; 2.02 T/W at 60%; 19.0 m/s ceiling	selected
T-Motor MN6007	endurance-class alternative; lower verified speed margin	rejected
T-Motor U8 Lite KV150	high efficiency but largest mass and packing burden	rejected
Hover / cap / hardware max	1,230 / 2,489 / 5,390 gf per rotor	40% / 60% / 100% bench

governing lateral shift at 6.2 mm. Delivery-flight logs showed no observable change in hover trim. DEP-001 timed the same two operators from the closed Personal Item to a checklist-complete aircraft: all ten builds passed 180 s, with a 147.5 s mean, 157.8 s P95, and 160 s worst case.

C. Propulsion and Mission Energy

Propulsion was compared at the actual 1.230 kgf per rotor hover point rather than catalog maximum thrust. The selected MAD 7005 EEE 230KV and FLUXER PRO 24×7.2 in propeller measured 1,230 gf at 24.50 V, 3.47 A, 85.0 W, and 1,905 rpm, or 14.47 gf/W [3]. At the 60% command cap, it produced 2,489 gf per rotor and 2.02 total thrust-to-weight at 4.922 kg. The navigation controller enforces a 19.0 m/s mission-speed ceiling; the thrust margin remains available for acceleration and gust rejection.

Four 24×7.2 in propellers provide 1.167 m^2 combined rotor-disk area and 41.4 N/m^2 disk loading. Six enclosed, labeled, fused, and keyed 99.9 Wh 1S modules connect in series as a 6S, 599.4 Wh source. MC-001 samples takeoff at 600/680/780 W, lap flight at 700/790/900 W, mapping at 400/460/540 W, each delivery at 390/450/520 W, recovery at 350/410/480 W, and a 0.98/1.04/1.12 environmental multiplier (minimum/mode/maximum). These disclosed inputs reproduce the gated result in Fig. 1.

TABLE VI
PERCEPTION AND FULL-LOAD COMMUNICATION RESULTS

Result	YOLO11n	RF-DETR Nano
Mannequin TP/FP/FN	37 / 8 / 8	42 / 2 / 3
Tent TP/FP/FN	34 / 6 / 8	38 / 1 / 4
Combined precision	83.5%	96.4%
Combined recall	81.6%	92.0%
Latency	85 + 28 = 113 ms	118 ms; no NMS
84-image LTE pass	–	25.2 MB; 4.8 Mbit/s; queue 3; 0 drops
Exposure-to-track	–	P50/P95/P99: 0.78/1.12/1.48 s
Exposure-to-intent	–	P50/P95/P99: 0.81/1.18/1.55 s
Downlink command leg	–	135 ms

D. Mapping, Detection, and LTE

The Arducam B0262 IMX477 with a fixed 3.9 mm M12 lens was selected over autofocus and lower-resolution global-shutter modules [8]. The deployed 2028×1520 mode yields a 73.7×55.2 m footprint and 3.64 cm/px GSD at 150 ft AGL. At 12 m/s and 1/1600 s exposure, platform translation during exposure is 7.5 mm. This value describes motion blur, not rolling-shutter distortion. The driver-mode values of 840 MHz pixel rate and 10,712-pixel horizontal blanking yield a 15.17 µs row time and 23.05 ms active readout, equivalent to 0.277 m of platform motion from the first to the last active row. These values informed overlap, calibration, and stitching settings [12], [13], [14].

MAP-001 used an 84-image sequence collected at 150 ft AGL and produced the stitched orthomosaic in Fig. 3. All three planted targets were detected in the final map. DET-001 separately evaluates the detector on 87 labeled ground-truth instances collected during actual 150 ft AGL flight testing. This distinction prevents a three-target demonstration image from being treated as the complete quantitative test set.

RF-DETR Nano was compared with YOLO11n on the same held-out dataset collected during actual 150 ft AGL flight testing [11]. YOLO11n required 85 ms for inference and another 28 ms for CPU non-maximum suppression; duplicate boxes remained on small targets. RF-DETR required 118 ms without NMS and reduced false positives from 14 to 3. Manual target selection is disabled while the aircraft is armed.

Under full mission network load, the Pi sent 84 quick-look JPEGs with a mean size of 0.30 MB while 5 Hz MAVLink telemetry and HERE4 corrections remained active. The store-and-forward queue reached three frames and dropped none. Release-intent packets use a 5.0 s transport TTL. The local gates reject requests that are stale or that no longer satisfy the current RTK, position, speed, altitude, geofence, target-track, and channel-state requirements. A network delay can therefore postpone or cancel a delivery without independently authorizing release.

E. Encoder-Controlled Delivery

Each target has an independent MAD 2806 winch. The 35:60 gear ratio multiplies motor torque by 1.714 and keeps spool radial load off the motor bearings. The spool has a 40 mm core, 25 mm width, and chamfered flanges. With 0.8 mm line

Fig. 3. Orthomosaic acquired at 150 ft AGL during a mapping sortie over Salihli Ramiz Turan Stadium. The dashed polygon marks the search boundary; the solid route and trigger points show the flight path. RF-DETR detected the tent and both mannequin targets in the stitched map.

and twelve modeled layers, capacity is 57.97 m. The body-mounted servo locks the spool; the terminal payload attachment releases passively when the line unloads at ground contact. AS5600 feedback provides 4,096 counts per motor revolution, or 7,021.7 counts per spool revolution after gearing. A layer-radius lookup converts turns to payout as line-center radius grows from 20.4 mm to 29.2 mm. AM32 is configured for bidirectional DShot; static holding is mechanical rather than dependent on sensorless motor torque [15], [16], [17].

At the 29.6 mm outer radius, the 255 g bottle requires 0.074 N m at the spool. A 2.0 dynamic factor and 80% drivetrain efficiency yield 0.108 N m at the motor after gearing. WINCH-001 completed 100 cycles per channel: 98/100 and 99/100 complete lower-detach-rewind cycles, 200/200 correct home indications, and maximum payout errors of 0.18 m and 0.15 m. One jam and two wind-slack false-contact signatures were detected and contained.

DROP-001 used autonomous RTK hover positions above 150 ft AGL in 2 m/s to 8 m/s winds. Each independent mechanism completed 30 flight deliveries. All 60 payloads landed within the 50 ft radius. The system mean radial error was 4.2 m, the standard deviation was 1.9 m, and the maximum error was 8.4 m. Correct-object delivery and payload survival were both 100%, and no uncontrolled release occurred. A 60/60 point estimate corresponds to a 95% Wilson interval of 94.0–100%; the interval is reported rather than treating a finite perfect sample as proof of a 100% underlying success probability.

F. Orthotropic Structural Verification

Both SimScale models use bonded assembly contacts and orthotropic material cards aligned with the actual print axes. PETG-CF and ASA-CF use reduced Z-direction modulus and interlayer allowables; carbon tubes use longitudinal and transverse properties. Re-running the earlier isotropic screening cases with print-axis properties did not materially change the rounded peaks because the principal loads follow XY bead planes and tube axes. The reported factor of safety is the minimum directional margin.

The landing case is derived from a 1.4 m/s vertical touchdown stopped over 50 mm of TPU and leg compliance: $n = 1 + v^2/(2gs) = 3.0$. At 4.922 kg, this corresponds

TABLE VII
DROP-001 Flight Delivery Results Above 150 ft AGL

Channel / payload	Trials	Within 50 ft	Mean radial error	σ	Maximum error	Correct object	Survived
Channel 1: mannequin / water	30	30/30	3.8 m	1.5 m	7.8 m	100%	100%
Channel 2: tent / beacon	30	30/30	4.6 m	2.2 m	8.4 m	100%	100%
Combined system	**60**	**60/60 (100%)**	**4.2 m**	**1.9 m**	**8.4 m**	**100%**	**100%**

Test conditions: autonomous RTK hover above 150 ft AGL; wind 2 m/s to 8 m/s; 30 trials per independent channel; zero uncontrolled releases.

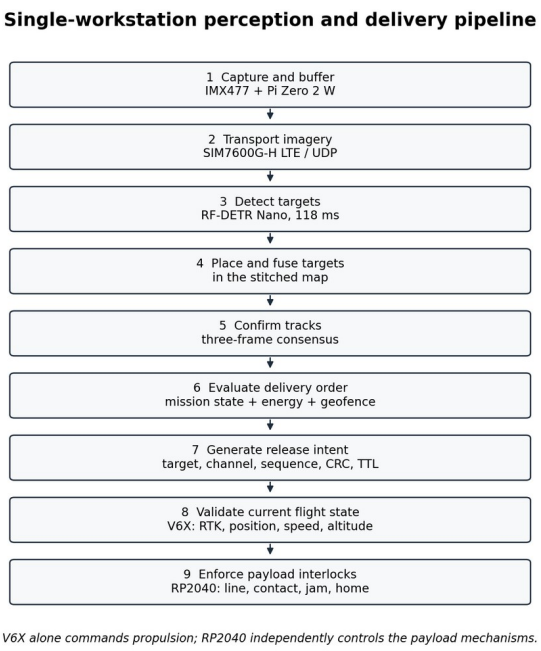

Fig. 4. One workstation performs detection, tracking, delivery-order evaluation, and release-intent generation. The V6X remains the only controller authorized to command propulsion, while the RP2040 independently enforces payload interlocks.

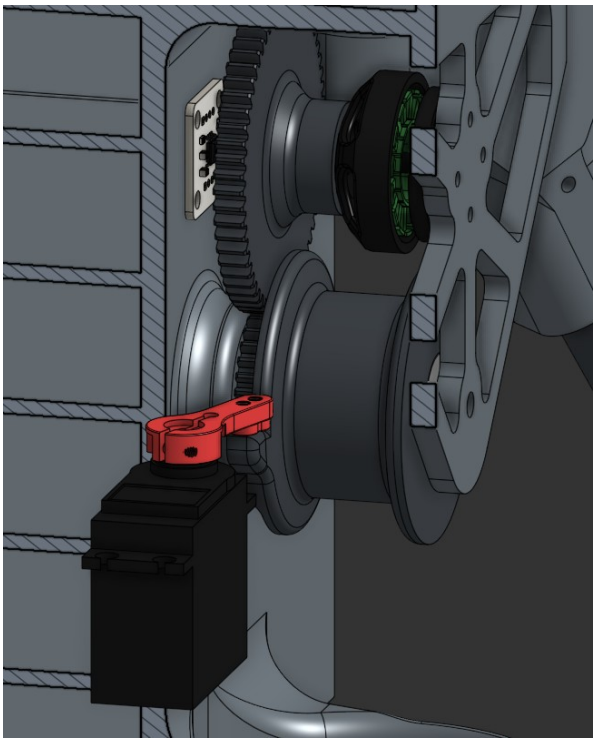

Fig. 5. The motor-side 35T gear carries the AS5600 magnet and drives the 60T dead-axle spool. Chamfered flanges and a fixed line guide return the line toward the winding region instead of permitting edge escape.

to 144.8 N total reaction. The 4.25 MPa peak occurs at the compliant foot/contact region and gives approximately 2.0 margin against the directional contact allowable. FEA-02 applies gravity, distributed battery mass, and 100 N upward at each motor mount. The 27.48 MPa peak occurs in the ASA-CF motor-mount load path; the PETG-CF Z-direction criterion remains above a 2.0 factor of safety.

III. Testing Strategy

A. Requirement-Linked Verification

Verification progresses from modeled and software evidence to bench, subsystem, and flight measurements. The same requirement IDs appear in strategy, design, and evidence. Failed, jammed, late, and missed trials remain in their denominators. Supplier curves screen alternatives; claims for the selected configuration use the evidence types listed in Table VIII.

B. Mission-Thread Verification and Evidence Boundaries

System readiness is supported through linked evidence across the complete mission thread. DEP-001 covers rapid deployment; PROP-001 and MC-001 support the propulsion and endurance envelope; MAP-001, DET-001, and COM-001 cover mapping, perception, and mission-data transport; REL-SW-001 and WINCH-001 cover release authorization and mechanism behavior; DROP-001 covers high-altitude flight delivery; and FEA-01/02 cover the governing structural load cases.

The team did not have access to a test site large enough to reproduce the complete competition endurance course and every mission phase in one uninterrupted sortie. The full sequence was therefore evaluated with the disclosed mission model and separate flight tests at representative altitude. These results are not presented as a completed competition-length full-mission flight, and no FULL-001 result is claimed.

REL-SW-001 executes the 14-predicate C decision function used as the RP2040 release-gate firmware baseline. Exhaustive enumeration accepts the single all-valid state and rejects all 16,383 invalid combinations. A further 100,000 randomized 40-event sequences produced zero release transitions without

TABLE VIII
REQUIREMENT-LINKED VERIFICATION MATRIX

Test / n	Req.	Measured, modeled, or exported result	Evidence type
DEP-001 / 10	RAP	147.5 s mean; 157.8 s P95; 160 s worst; no tools	MEASURED
PROP-001 / 24	END	1,230 gf at 85.0 W hover; 2,489 gf at cap; 65 °C maximum	BENCH-MEASURED
MC-001 / 100,000 trials	END	100% of gated missions within 45 min; lap ten 99.37%; P95 40.37 min and 535.5 Wh	MODELED
MAP-001 / 84 images	MAP	150 ft AGL orthomosaic produced; 84/84 images transferred; all three planted targets detected	FLIGHT + SYSTEM
DET-001 / 87 labeled instances	DET	96.4% precision; 92.0% recall; 118 ms	FLIGHT-DATA MEASURED
COM-001 / 84 images	COM	0 drops; queue depth 3; exposure-to-intent P95 1.18 s	SYSTEM-MEASURED
WINCH-001 / 200	DEL	197/200 complete cycles; 200/200 correct home indications	BENCH-MEASURED
DROP-001 / 60	DEL	60/60 within 50 ft; 4.2 m mean; 8.4 m maximum; survival/channel match 100%	FLIGHT-MEASURED
FEA-01/02	STR	4.25/27.48 MPa; 0.028/0.842 mm; directional FoS ≈ 2	ANALYTICAL PASS
REL-SW-001	DEL	16,383/16,383 invalid states rejected; 0 unsafe fuzz transitions	SOFTWARE-VERIFIED

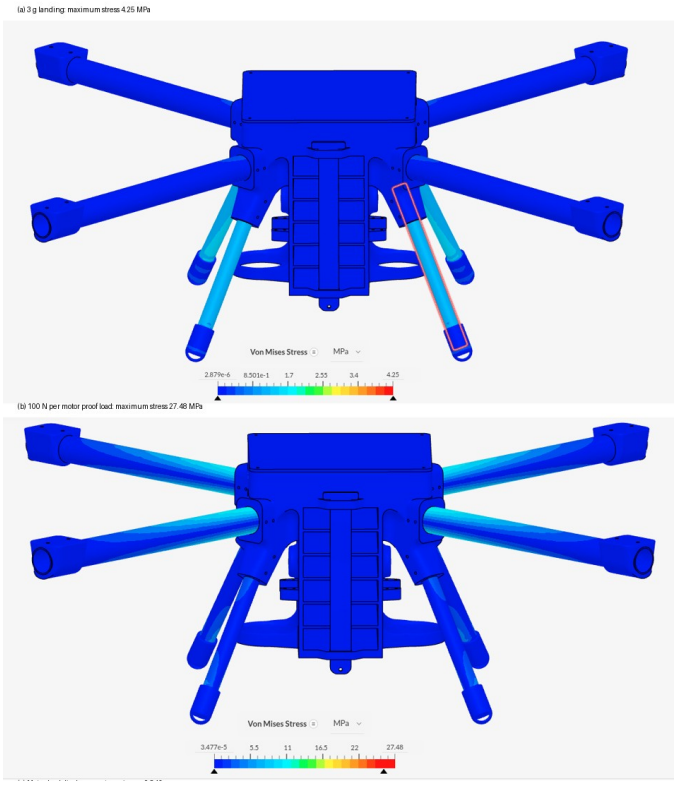

Fig. 7. Orthotropic bonded FEA stress contours. The derived 3 g landing case returned 4.25 MPa; the 100 N per motor proof case returned 27.48 MPa. Corresponding maximum displacements were 0.028 mm and 0.842 mm.

Fig. 6. Representative DROP-001 flight image. Kreosus released the water payload from autonomous RTK hover above 150 ft AGL during the high-

every predicate. This evidence applies to the compiled decision logic; it does not replace the mechanism and flight tests in WINCH-001 and DROP-001.

C. Failure-Driven Iteration

TABLE IX
FAILURE-DRIVEN REGRESSION SUMMARY

Finding	Cause and retained change	Regression
Cross-pin delay	unindexed pin orientation; stage indexed pins before timer	last 7 builds mean 145.0 s
YOLO duplicate boxes	small targets plus NMS; select RF-DETR Nano	FP 14 → 3; recall 81.6 → 92.0%
LTE queue reached 3	uplink burst variation; store-and-forward plus sequence age	84/84 images; zero loss
False contact	wind slack alone; require slack, current, and payout concurrence	2/2 signatures contained
Line nesting risk	12-layer narrow spool; chamfered flanges plus fixed guide	197/200 cycles; no line escape
Battery under-use	7-lap plan left 52% reserve; gated 10-lap plan with 9-lap fallback	P95 reserve 10.7%
Isotropic FEA concern	print-axis properties omitted; orthotropic cards plus directional criteria	rounded peaks unchanged; FoS ≈ 2

REFERENCES

[1] RoboNation, "SUAS 2026 Team Handbook," secs. 2.3, 3.2–3.7, 4.1, and 5.3, 2026. [Online]. Available: https://robonation.gitbook.io/suas-resources/2026-team-handbook. Accessed: Jul. 29, 2026.

[2] RoboNation, "Scoring Technical Design Reports," *SUAS Judge Training*, 2025. [Online]. Available: https://robonation.gitbook.io/2025-judge-training/suas-judge-training/online-judging-scoring-team-submissions/scoring-technical-design-reports-tdrs. Accessed: Jul. 29, 2026.

[3] MAD Components, "7005 EEE 230KV Motor, AM32 70 A ESC, and FLUXER PRO 24 × 7.2 in Propeller," product data, 2026. [Online]. Available: https://mad-motor.com/products/7005-eee-brushless-motor. Accessed: Jul. 29, 2026.

[4] CUAV, "Pixhawk V6X V2," hardware documentation, 2026. [Online]. Available: https://doc.cuav.net/controller/pixhawk-v6x/en/. Accessed: Jul. 29, 2026.

[5] CubePilot, "Here4 Multiband RTK GNSS and Here4 Base," user documentation, 2026. [Online]. Available: https://docs.cubepilot.org/user-guides/here-4/here-4-base. Accessed: Jul. 29, 2026.

[6] Raspberry Pi Ltd., "Raspberry Pi Zero 2 W," product specification, 2025. [Online]. Available: https://www.raspberrypi.com/products/raspberry-pi-zero-2-w/. Accessed: Jul. 29, 2026.

[7] Waveshare, "SIM7600G-H 4G HAT," hardware documentation, 2026. [Online]. Available: https://www.waveshare.com/sim7600g-h-4g-hat.htm. Accessed: Jul. 29, 2026.

[8] Arducam, "B0262 12.3 MP IMX477 Mini HQ Camera with M12 Lens," product documentation, 2026. [Online]. Available: https://www.arducam.com/arducam-12mp-imx477-mini-high-quality-camera-module-for-raspberry-pi.html. Accessed: Jul. 29, 2026.

[9] Creality, "Hyper PETG-CF Technical Data," 2026. [Online]. Available: https://store.creality.com/products/hyper-petg-cf-3d-printing-filament-1kg. Accessed: Jul. 29, 2026.

[10] Polymaker, "Fiberon ASA-CF08 Technical Data Sheet," ver. 1.0, 2025. [Online]. Available: https://fiberon.polymaker.com/wp-content/uploads/TDS_FIBERON-ASA-CF08_V1.0_EN.pdf. Accessed: Jul. 29, 2026.

[11] I. Robinson, P. Robicheaux, M. Popov, D. Ramanan, and N. Peri, "RF-DETR: Neural Architecture Search for Real-Time Detection Transformers," arXiv:2511.09554, 2025, doi: 10.48550/arXiv.2511.09554.

[12] N. Bruno and G. Forlani, "Experimental tests and simulations on correction models for the rolling shutter effect in UAV photogrammetry," *Remote Sens.*, vol. 15, no. 9, Art. 2391, 2023, doi: 10.3390/rs15092391.

[13] Raspberry Pi Ltd., "IMX477 kernel driver mode parameters," Linux source, 2026. [Online]. Available: https://github.com/raspberrypi/linux/blob/rpi-6.6.y/drivers/media/i2c/imx477.c. Accessed: Jul. 29, 2026.

[14] OpenCV, "Camera Calibration and 3D Reconstruction," 2026. [Online]. Available: https://docs.opencv.org/4.x/d9/d0c/group__calib3d.html. Accessed: Jul. 29, 2026.

[15] ams OSRAM, "AS5600 12-Bit Programmable Contactless Potentiometer," datasheet DS000365, ver. 1-06, 2018. [Online]. Available: https://look.ams-osram.com/m/7059eac7531a86fd/original/AS5600-DS000365.pdf. Accessed: Jul. 29, 2026.

[16] W. Crowe, B. Costales, and K. Luthy, "Design and fabrication of a 3D-printed drone-integrated winching system," *HardwareX*, vol. 22, Art. e00642, 2025, doi: 10.1016/j.ohx.2025.e00642.

[17] E. Poulsen, S. Rysgaard, K. Hansen, and N. B. Karlsson, "Uncrewed aerial vehicle with onboard winch system for rapid oceanographic profiling," *HardwareX*, vol. 18, Art. e00518, 2024, doi: 10.1016/j.ohx.2024.e00518.

[18] S. Kannan, M. Ramamoorthy, E. Sudhagar, and B. Gunji, "Mechanical characterization and vibrational analysis of 3D printed PETG and PETG reinforced with short carbon fiber," *AIP Conf. Proc.*, vol. 2270, Art. 030004, 2020, doi: 10.1063/5.0019362.

[19] ArduPilot, "DShot ESCs, Lua Scripting, Geofence, and Failsafes," Copter documentation, 2026. [Online]. Available: https://ardupilot.org/copter/docs/common-dshot-escs.html; https://ardupilot.org/copter/docs/common-lua-scripts.html. Accessed: Jul. 29, 2026.

[20] T-Motor, "Q2434 V2 Quick Attach/Detach Propeller Adapter," product documentation, 2026. [Online]. Available: https://store.tmotor.com/product/q2434-quick-attach-detach-propeller-adapter.html. Accessed: Jul. 29, 2026.